NANO LETTERS

2007
Vol. 7, No. 12
3698−3703

Fluorescence Efficiency of Individual Carbon Nanotubes

Lisa J. Carlson,[†] Sara E. Maccagnano,[‡] Ming Zheng,[§] John Silcox,[‡] and Todd D. Krauss*,[†]

Chemistry Department, University of Rochester, Rochester, New York 14627, School of Applied Engineering Physics, Cornell University, Ithaca, New York 14853, and DuPont Central Research and Development, Experimental Station, Wilmington, Delaware 19880

Received August 12, 2007; Revised Manuscript Received October 8, 2007

ABSTRACT

The luminescence efficiency of individual single-walled carbon nanotubes was determined by comparing the fluorescence from individual nanotubes to single CdTe/ZnS quantum dots with a well-defined fluorescence quantum yield (QY). The single carbon nanotube QY was determined to be 3 ± 1%, nearly 100 times greater than values previously reported for ensembles. The intrinsic nanotube QY is potentially much higher than previously believed and appears lower in ensembles due to defective nanotubes and residual bundles.

Single-walled carbon nanotubes (SWNTs) possess an impressive array of optical properties, including size-tunable emission,[1] near-infrared fluorescence,[2] and high photostability.[3,4] These qualities are extremely desirable for fluorescence-based applications such as biological imaging[4,5] and biological sensing,[6] which rely heavily upon the availability of fluorophores with high brightness and stable emission. Nanotubes may also fulfill the long-standing need for a single-photon source in the near-infrared, which is necessary for applications in quantum optics.[7]

Because they experience strong van der Waals attractions, nanotubes form aggregated bundles when synthesized. This interaction quenches SWNT fluorescence by allowing nonradiative transfer from semiconductor SWNTs to any metallic nanotubes within the bundle.[2] A major milestone in the optical characterization of SWNTs was the development of an ultrasonic dispersion method to wrap surfactants around nanotubes, thereby isolating them.[2] Fluorescence spectra of isolated SWNTs exhibit a series of well-resolved peaks that correspond to optical transitions from various (*n*,*m*) structures present within an ensemble,[1,8] as displayed in the inset to Figure 1a.

Toward the realization of applications based on nanotube fluorescence, one important consideration is their relative fluorescence efficiency, or fluorescence quantum yield (QY). Based on a ratio of radiative and nonradiative rate constants, a molecule's QY is also one of its most fundamentally important photophysical parameters.[9] For an ensemble of nanotubes, the fluorescence QY is <0.05%,[2,10,11] which is extremely poor and would likely preclude their use in fluorescence-based applications. However, recent experiments suggest that the QY of SWNTs is potentially much higher than previously reported. For example, unusually fast excited-state recovery times suggest that a significant fraction of suspended nanotubes are bundled and, therefore, nonemissive.[12] In addition, the fluorescence from single nanotubes can be detected with high signal-to-noise, suggesting a higher QY for individual nanotubes.[3] In another study, when SWNTs were suspended with a density gradient and subsequently fractionated,[13] the least dense fractions showed QYs of ∼1%.[14] Finally, the absolute QY for nanotubes suspended across pillars was recently estimated to be ∼7%,[15] but the accuracy of such measurements is limited by difficulties in knowing the exact number of photons absorbed by the sample and received by the detector, which are extremely challenging to quantify.

Here we present measurements of the fluorescence QY of isolated SWNTs obtained using single molecule spectroscopy. Comparisons between the relative fluorescence intensities of individual SWNTs and CdTe quantum dots (QDs) allowed for a direct determination of the QY for bright nanotubes (QY ∼ 3 ± 1%), which is 2 orders of magnitude higher than the value for ensembles. This approach offers the first relative fluorescence QY measurement on the single particle level and allows us to report on whether the measured ensemble SWNT QY represents an intrinsic property of all nanotubes. Our measurements can also determine the influ-

* Corresponding author. E-mail: Krauss@chem.rochester.edu.
[†] University of Rochester.
[‡] Cornell University.
[§] DuPont Central Research and Development.

10.1021/nl072014+ CCC: $37.00
Published on Web 11/13/2007

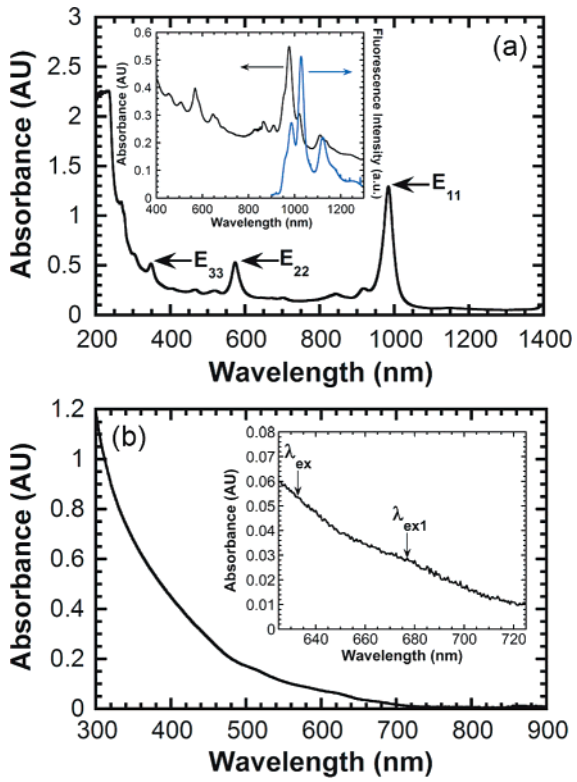

Figure 1. (a) Absorption spectrum from a DNA-solubilized SWNT sample, highly enriched in (6,5) nanotubes (1 cm path length). The first, second, and third excited excitonic states are labeled in the figure. Inset: absorption and fluorescence spectra ($\lambda_{ex} = 632.8$ nm, excitation intensity ~ 28 mW/cm^2, 500 ms integration time at each data point) from an ensemble of isolated CoMoCAT carbon nanotubes. (b) Absorption spectrum for 705 ITK CdTe/ZnS QDs. Inset: absorption spectrum with the excitation wavelength ($\lambda_{ex} = 632.8$ nm) and first exciton absorption peak ($\lambda_{ex1} \sim 677$ nm) indicated.

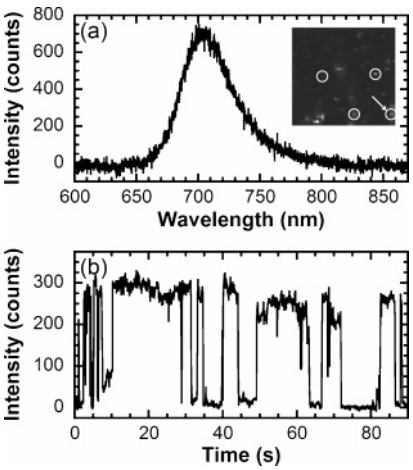

Figure 2. (a) Single CdTe/ZnS QD fluorescence spectrum. Inset: 2D fluorescence image of a 20 × 20 μm^2 area scanned with an $\sim$1.5 kW/cm^2 intensity. Circled pixels indicate fluorescence from individual nanoparticles (top two circles correspond to SWNTs and bottom two circles correspond to QDs). The spectrum corresponds to the circled pixels indicated with an arrow. (b) Time trace for the same QD showing the characteristic on/off blinking behavior, which confirms that the spectrum corresponds to a single molecule.

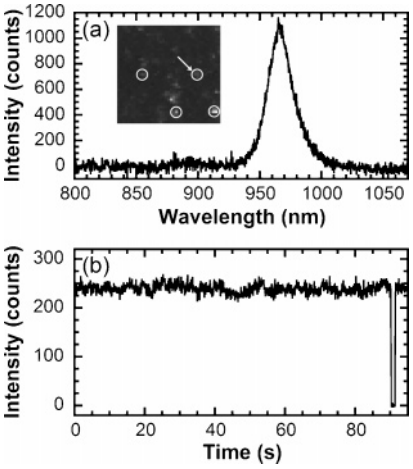

Figure 3. (a) Typical fluorescence spectrum from an (8,3) SWNT. Inset: 2D fluorescence image of the same 20 × 20 μm^2 area in Figure 2, scanned with an $\sim$30 kW/cm^2 intensity. Emission from a single (8,3) SWNT corresponds to the circled pixels indicated with an arrow. (b) Time trace for the same SWNT showing stable and uninterrupted emission over 95 s. The laser was physically blocked to artificially produce the off level of fluorescence near the end of the scan.

ence of inter-tube interactions (i.e., residual bundles), processing defects, or interactions with the local environment on the QY.

For fluorescence measurements, CoMoCAT-manufactured SWNTs (SouthWest Nanotechnologies, Inc.) were dispersed with sodium cholate in D_2O using methods similar to O'Connell et al.[2] Carboxyl-coated ITK 705 CdTe/ZnS quantum dot samples (Invitrogen Corporation) were diluted with water to $\sim$0.1 nM. SWNTs and QDs were then spun cast consecutively onto a quartz cover slip.

Fluorescence from SWNTs and QDs was accomplished by epifluorescence microscopy on an inverted microscope, using a helium−neon laser for excitation ($\lambda_{ex} = 632.8$ nm) through a 100× oil immersion objective (NA = 1.3). Emission was collected by the same objective and passed through two holographic notch filters before reaching a cooled Si:CCD detector. A piezoelectric scanning stage was used to create a 2D image representative of the fluorescence from the sample, with typical images shown in the insets of Figures 2 and 3. The excitation intensity was $\sim$1.5 kW/cm^2 ($\sim$30 kW/cm^2) for QDs (SWNTs). The stage could be positioned to place a single nanoparticle in the excitation beam, allowing collection of fluorescence spectra and time traces (temporal changes in intensity under continuous excitation) with typical integration times of 1 min and 100 ms, respectively.

Scanning transmission electron microscopy (STEM) with electron energy loss spectroscopy (EELS) was used to determine the chemical distribution of core and shell atoms in the CdTe/ZnS QDs[16] (705 ITK organic quantum dots, Invitrogen Corporation). STEM images were collected using the Cornell VG HB501 100 kV UHV STEM, and EELS data were obtained as described previously.[16] The SWNT cross section was calculated from the absorption spectrum of a sample highly enriched in (6,5) SWNTs, shown in Figure 1a.[17]

Table 1. Raw Fluorescence Intensities for SWNTs and QDs

	(6,4) SWNTs	(9,1) SWNTs	(8,3) SWNTs	(6,5) SWNTs	CdTe/ZnS QDs
E_{22} (nm)[a]	581	693	663	567	-
E_{11} (nm)[a]	873	912	952	975	-
av fluorescence intensity (counts)[b]	196	188	203	183	263
counts/power (counts/mW)	153	147	159	143	2023
av QY (%)	3.1	2.9	3.0	2.9	-
estimated $\sigma_{633\,nm}$ (cm^2)[c]	7×10^{-15}	7×10^{-15}	7.5×10^{-15}	7×10^{-15}	2.6×10^{-15}
σ_{E11} (cm^2)[c]	-	-	-	1×10^{-13}	-

[a] Literature values.[1] [b] Fluorescence intensities were later corrected by the excitation intensity and detection efficiency at the peak emission wavelength. [c] The absorption cross section was measured for enriched (6,5) SWNTs and was used to estimate approximate values for all other chiralities in this study.

A molecule's relative QY is typically determined by comparing the spectrally integrated fluorescence intensity of the unknown to a molecule with a known QY. For example, for the CoMoCAT SWNTs in sodium cholate, an ensemble fluorescence QY of ~0.03% was determined via direct comparison with the standard infrared dye IR-26 ($\lambda_{ex} = 900$ nm, intensity ~ 37 mW/cm^2, 600 ms integration time at each data point). However, there is no well-established procedure that has been used to determine the relative fluorescence QY for a single molecule. We have defined the single nanotube relative QY by eq 1, which is comparable to an expression given by Lakowicz.[18]

$$\Phi_{SWNT} = \Phi_{QD}\left(\frac{F_{SWNT}}{F_{QD}}\right)\left(\frac{\sigma_{QD}}{\sigma_{SWNT}}\right)\left(\frac{I_{QD}}{I_{SWNT}}\right)\left(\frac{\eta_{QD}}{\eta_{SWNT}}\right) \quad (1)$$

Φ is the fluorescence quantum yield, F is the fluorescence intensity, σ is the molecular absorption cross section, I is the excitation intensity, and η is the efficiency of the detector at the emission wavelength. In an ensemble QY measurement, the fluorescence intensities are corrected by the absorbance at the excitation wavelength for each sample.[18] Here, we correct the fluorescence counts for the relative excitation rate of the two nanoparticles using the product of absorption cross section and excitation intensity.[18]

CdTe QDs are an ideal reference molecule for our measurement for several reasons. First, the single molecule fluorescence QY is very well defined for CdSe QDs (closely related to CdTe QDs). Indeed, correlated AFM and fluorescence imaging,[19] fluorescence correlation spectroscopy,[20] and dielectric-dependent photoluminescence studies[21] have all demonstrated that the fluorescence QY approaches unity for individual bright QDs. Therefore, although the ensemble CdTe QD QY is ~70%, we can assume that the maximum fluorescence counts in a given time trace correspond to a single CdTe QD QY of ~100%. Second, the fluorescence from individual QDs is very robust, and thus there exists little chance that the QD will irreversibly photobleach during the course of the measurement. Finally, these CdTe QDs absorb and fluoresce at wavelengths in the near-infrared, and so they can be excited by the same laser source used for the SWNTs.

A fluorescence spectrum from a single CdTe/ZnS QD with emission centered at ~705 nm and a fwhm of ~40 nm is displayed in Figure 2a, with a typical fluorescence image shown in the inset. The characteristic fluorescence intermittency, or on/off blinking behavior, for emission from a single quantum dot is shown in Figure 2b. Blinking is considered to be a definitive hallmark of fluorescence from a single QD,[22] and time traces were collected for each nanoparticle to confirm that individual QDs were being studied.

The corresponding image and spectrum of the fluorescence from a single nanotube are shown in Figure 3a. For single SWNTs, the emission follows a Lorentzian line shape with energies corresponding to E_{11} transitions of particular nanotube (n,m) structures and also exhibits a narrow line width limited by ~k_BT at room temperature.[3] A time trace collected for this same nanotube is presented in Figure 3b and illustrates the continuous, photostable emission of SWNTs, in stark contrast to what is observed for single QDs. Because light absorption is not strongly allowed for nanotubes that lie perpendicular to the polarization axis of the excitation source,[3,23−25] the nanotubes we observe are oriented nearly parallel to the exciting electric field. The raw fluorescence intensities collected for QDs and SWNTs are summarized in Table 1.

Determining an accurate absorption cross section for QDs and SWNTs is critical to determining their excitation rates. For II−VI QDs, the absorption cross section can be related to the size of the QD.[26,27] From the first exciton absorption wavelength, the diameter of the CdTe QD can be calculated using an empirical fitting function,[27] which can then be used to calculate the absorption cross section at the first exciton absorption peak.[26,27] For the CdTe/ZnS QDs, the first exciton absorption peak resides at ~677 nm (Figure 1b), corresponding to a CdTe core diameter of ~55 Å and a cross section of ~1.43×10^{-15} cm^2. However, large red shifts by as much as 130 nm have been observed upon capping CdTe QDs with a semiconductor shell[28] and, therefore, it is unclear whether the position of the absorption peak can be used to determine the cross section reliably. Further, these QDs are highly anisotropic and exhibit a characteristic bullet shape,[29] which complicates the direct determination of the QD diameter based on simple empirical formulas.

Therefore, for high accuracy, STEM with EELS imaging was employed to accurately quantify the dimensions of the emissive CdTe core. Figure 4 displays an annular darkfield (ADF) scattering image for a typical CdTe/ZnS QD acquired by STEM. The ADF signal is proportional to the sample thickness and the atomic number of the imaged material (to

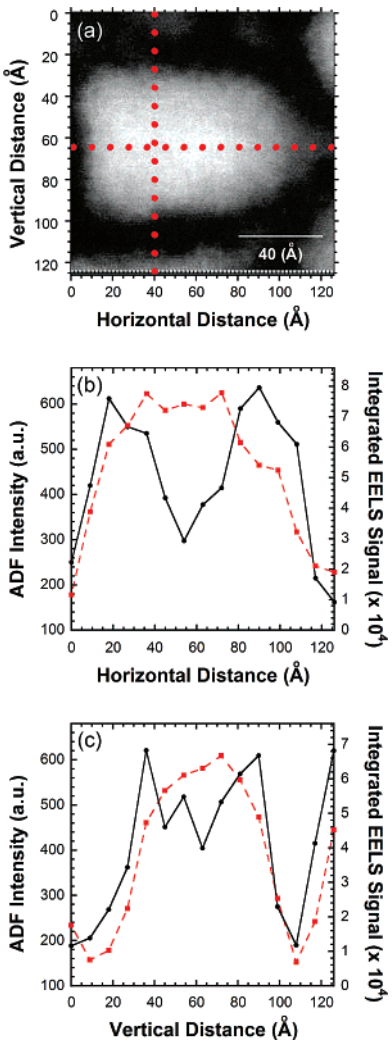

Figure 4. (a) Annular darkfield STEM image for a typical single CdTe/ZnS QD. The red horizontal and vertical dots correspond to the data points in (b) and (c), respectively, and indicate the positions along the dot for which ADF and EELS data were collected. (b) ADF (dashed red line, squares) and integrated EELS (solid black line, circles) data were acquired by scanning across the QD horizontally. The length of this CdTe QD core is approximately 61 Å. (c) ADF (dashed red line, squares) and integrated EELS (solid black line, circles) data were acquired by scanning across the QD vertically. The width of this CdTe core is approximately 51 Å.

the power of ~1.7).[30] Conversely, the integrated EELS signal for sulfur (a component of the shell material) is proportional to the amount of sulfur in the direction of electron beam propagation.[16] For a well-shaped QD, the integrated EELS signal generally displays a maximum at the edges of the core, where the total cross-sectional shell thickness is greatest, and a minimum at the center of the core, where the total shell thickness is smallest.

Atomic EELS imaging is very difficult, and data were collected for 7 QDs. From theoretical modeling of the EELS signals, we determined the distribution of the shell around the core, and thus could determine an average core length of 67.5 ± 2.9 Å and a core diameter of 47.9 ± 1.7 Å. Using a weighted average to obtain an effective QD diameter (to insert into the empirical expressions), these values translate to an absorption cross section at the first exciton absorbance of 1.4×10^{-15} cm^2, in excellent agreement with our optical measurement. At the excitation wavelength, the QD absorbance is nearly 2 times greater than at the first exciton peak (Figure 1b). Hence, the absorption cross section (σ_{QD}) at 633 nm is $\sim 2.6 \times 10^{-15}$ cm^2 (Table 1).

The SWNT cross section was calculated from the absorption spectrum of a sample of highly enriched (6,5) DNA−SWNTs, shown in Figure 1a. To determine the mass of SWNTs present in a 1 mL solution containing ~20 μg of combined DNA and SWNTs, the mass of DNA was determined by subtracting the SWNT contribution under the DNA absorption peak ($\lambda \sim 270$ nm) according to Nair et al.[31] We determined that ~12 μg of (6,5) SWNTs are present, in good agreement with the molecular modeling predictions of a DNA:SWNT mass ratio of 1:1.[32] The SWNT concentration was converted to a molarity ($\sim 2.5 \times 10^{-8}$ M) by quantifying the number of moles of carbon present in a 380 nm long SWNT.[33] This SWNT length, as measured by AFM, is typical of our samples and agrees with length distributions for other samples prepared by ultrasonic dispersion methods.[34,35] In general, Beer's law can be used to extract the density of SWNTs from the absorption spectrum of a single (n,m) SWNT species if its absorption cross section is known. Assuming a negligible difference in cross section among different SWNT structures, the concentration distribution for an ensemble of SWNTs can be extracted by a deconvolution algorithm that breaks an SWNT absorption spectrum into its (n,m) components[31] or by using experimentally determined calibration curves for a given surfactant.[36]

It is possible that some of the absorbance at 633 nm (Figure 1a) corresponds to impurities and not to the (6,5) nanotube. When detecting fluorescence from only the (6,5) SWNT (at ~990 nm), the relative ratio of the photoluminescence excitation (PLE) intensities at E_{22} and 633 nm serves to quantify the fraction of the sample that absorbs at 633 nm and also contributes to (6,5) nanotube fluorescence (assuming the absorption at E_{22} is all from (6,5) SWNTs). From the absorption spectrum, E_{22}:633 nm is ~2.5, and from the PLE spectrum, E_{22}:633 nm is ~4.9. Therefore, nearly half of the material absorbing at 633 nm is not contributing to the fluorescence at E_{11}, making the value of the SWNT cross section at 633 nm $\sigma_{SWNT} \sim 7 \times 10^{-15}$ cm^2, compared to a value of $\sigma_{SWNT} \sim 1 \times 10^{-13}$ cm^2 at E_{11} (Table 1).

Combining the measured absorption cross sections and the fluorescence intensities from individual SWNTs and QDs, we determined the average QY of individual isolated SWNTs to be ~3 ± 1%, nearly 100× greater than the ensemble value. This QY value represents an average over all SWNTs, including several different (n,m) structures that compose the CoMoCAT ensemble; the fluorescence intensity can vary by a factor of 2 from one individual SWNT to another. The value of the (6,5) SWNT cross section was assumed to be similar to other structures and, therefore, was used to calculate all QYs (Table 1). The authors emphasize that the QY represents the measured value for the brightest SWNTs in a sample, as single molecule fluorescence measurements are naturally biased toward molecules that exhibit the strongest fluorescence. In fact, recent single molecule pho-

tothermal absorption studies suggest that luminescent SWNTs comprise only a small fraction of all nanotubes in such a sample.[37]

The primary sources of error in the QY value arise from the variability in counts for each SWNT (~50%), as well as the determination of QD diameter (8%) and SWNT length (10−15%) in the respective calculated absorption cross sections. It is also unclear how the QY varies with SWNT length, which is a subject of current debate. For example, Fagan et al. have observed a strong dependence of fluorescence intensity of nanotube length[38] that is supported by another study showing an exciton diffusion length of ~90 nm along the SWNT.[39] These studies imply that the fluorescence efficiency for short SWNTs may be lowered by efficient quenching of bound excitons at the cut ends of nanotubes. However, because the average length of the nanotubes used here is over 350 nm, it is unlikely that pure length effects could change the QY value appreciably. Differences in the SWNT QY may arise for different lengths because shorter nanotubes likely have more defects as a result of the sonication process used to isolate them.

In principle, measurements of the QY relative to a known standard are much more straightforward than absolute QY measurements. In particular, it is extremely difficult to quantify, with a high degree of accuracy, the exact amount of light absorbed by the sample and received by the detector in an absolute QY measurement, especially on the single molecule level. The significance of our approach lies in the simplicity of correcting easily measured relative fluorescence intensities (between the reference molecule and the unknown) for the molecular absorption cross sections, excitation intensities, and detection efficiencies, all of which can be determined in a relatively simple manner with fairly high accuracy.

Because the individual SWNT QY is nearly 2 orders of magnitude greater than the ensemble value, the majority of nanotubes in an ensemble are either quenched in bundles or are not optically active (i.e., dark). Indeed, strong evidence that bundling is a major contributor to the low QY comes from ensemble fluorescence measurements on isolated SWNTs, which had a QY approaching 1% when separated from small bundles.[14] On the other hand, AFM studies of the dispersed SWNT sample find largely individual SWNTs,[40] suggesting that a significant fraction of the suspended individual nanotubes are dark. As noted, defects to SWNT sidewalls[41] and at the SWNT ends[42] that are introduced during the harsh sonication process can efficiently quench fluorescence and may explain the low percentage of bright nanotubes in an ensemble. However, the overall effect of structural imperfections on SWNT fluorescence efficiencies remains an important question in nanotube photophysics.

It is well-known that the local environment can affect the fluorescence energy and efficiency of SWNTs,[3] and it has been shown that SWNT fluorescence is quenched when the nanotube lies on a surface.[25] Interestingly, we have discovered that nanotubes deposited onto a quartz substrate are emissive, with a QY similar to that of purely suspended SWNTs.[15] Although it is possible that the micelle layer encapsulating the SWNT insulates it from the quartz surface, it is clear that surface-bound SWNTs do exhibit strong fluorescence, which should encourage further single nanotube optical studies using this relatively simple sample preparation method.

The maximum possible QY for SWNTs is still very much unknown, as a pristine SWNT free of the defects caused by harsh sonication and acidic purification processes may have a significantly higher QY than what we have measured. On the other hand, suspended SWNTs that are not subject to harsh sonication treatments seem to have QYs similar to the processed SWNTs we have measured.[15] This finding suggests that a perfect SWNT may have a QY only on the order of a few percent, limited by intrinsic nonradiative decay mechanisms such as phonon emission, or intersystem crossing to a triplet state or a low-lying nonradiative electronic state (e.g., dark exciton).[43,44]

Theory predicts that an optically forbidden exciton state, known as the dark exciton, lies just below the energy of the optically active exciton that is responsible for fluorescence.[43−45] However, the energetic separation of the bright (i.e., emissive) and dark exciton was recently determined to be only 5−10 meV, well within k_BT at room temperature.[46] The existence of the dark exciton may explain the low fluorescence efficiency of SWNTs relative to more efficient nanoparticles like single QDs. Indeed, recent studies show that the SWNT fluorescence lifetime decreases at low temperatures, suggesting that the dark exciton state may influence the radiative decay kinetics.[47] However, the role of the dark exciton in SWNT fluorescence remains an open question, and it certainly cannot account for the extremely low ensemble nanotube fluorescence QY relative to the single SWNT.

In conclusion, using an original single molecule method, we have determined that the QY for an individual SWNT is a few percent, which indicates that nanotubes' emissive efficiencies may not be as low as previously thought. Carbon nanotubes remain promising candidates for biological imaging, single molecule sensing, and quantum optics, and each of these applications would benefit greatly from the incorporation of SWNTs with a luminescence efficiency that is not impractically small. It is unclear just what limits the QY of individual SWNTs to a few percent, but further improvements in sample preparation and purification should allow for the eventual mitigation of fluorescence quenching due to defects, thereby allowing for further insights into intrinsic nanotube photophysics.

Acknowledgment. We thank the following for their financial support: the Camille Dreyfus Teacher−Scholar Awards Program, the Sloan Foundation, and the Department of Energy Office of Basic Energy Sciences.

References

(1) Bachilo, S. M.; Strano, M. S.; Kittrell, C.; Hauge, R. H.; Smalley, R. E.; Weisman, R. B. *Science* **2002**, *298*, 2361−2366.
(2) O'Connell, M. J.; Bachilo, S. M.; Huffman, C. B.; Moore, V. C.; Strano, M. S.; Haroz, E. H.; Rialon, K. L.; Boul, P. J.; Noon, W. H.; Kitrell, C.; Ma, J.; Hauge, R. H.; Weisman, R. B.; Smalley, R. E. *Science* **2002**, *297*, 593−596.

(3) Hartschuh, A.; Pedrosa, H. N.; Novotny, L.; Krauss, T. D. *Science* **2003**, *301*, 1354−1356.
(4) Heller, D. A.; Baik, S.; Eurell, T. E.; Strano, M. S. *Adv. Mater.* **2005**, *17*, 2793−2799.
(5) Cherukuri, P.; Gannon, C. J.; Leeuw, T. K.; Schmidt, H. K.; Smalley, R. E.; Curley, S. A.; Weisman, R. B. *Proc. Natl. Acad. Sci. U.S.A.* **2006**, *103*, 18882−18886.
(6) Barone, P. W.; Baik, S.; Heller, D. A.; Strano, M. S. *Nat. Mater.* **2004**, *4*, 86−92.
(7) Hartschuh, A.; Pedrosa, H. N.; Peterson, J.; Huang, L.; Anger, P.; Qian, H.; Meixner, A. J.; Steiner, M.; Novotny, L.; Krauss, T. D. *Chem. Phys. Chem.* **2005**, *6*, 577−582.
(8) Weisman, R. B.; Bachilo, S. M. *Nano Lett.* **2003**, *3*, 1235−1238.
(9) Fery-Forgues, S.; Lavabre, D. *J. Chem. Educ.* **1999**, *76*, 1260−1264.
(10) Huang, L.; Pedrosa, H. N.; Krauss, T. D. *Phys. Rev. Lett.* **2004**, *93*, 017403.
(11) Jones, M.; Engtrakul, C.; Metzger, W. K.; Ellingson, R. J.; Nozik, A. J.; Heben, M. J.; Rumbles, G. *Phys. Rev. B* **2005**, *71*, 115426.
(12) Huang, L.; Krauss, T. D. *Phys. Rev. Lett.* **2006**, *96*, 057407.
(13) Arnold, M. S.; Stupp, S. I.; Hersam, M. C. *Nano Lett.* **2005**, *5*, 713−718.
(14) Crochet, J.; Clemens, M.; Hertel, T. *J. Am. Chem. Soc.* **2007**, *129*, 8058−8059.
(15) Lefebvre, J.; Austing, D. G.; Bond, J.; Finnie, P. *Nano Lett.* **2006**, *6*, 1603−1608.
(16) Yu, Z.; Guo, L.; Du, H.; Krauss, T.; Silcox, J. *Nano Lett.* **2005**, *5*, 565−570.
(17) Zheng, M.; Jagota, A.; Strano, M. S.; Santos, A. P.; Barone, P.; Chou, S. G.; Diner, B. A.; Dresselhaus, M. S.; Mclean, R. S.; Onoa, G. B.; Samsonidze, G. G.; Semke, E. D.; Usrey, M.; Walls, D. J. *Science* **2003**, *302*, 1545−1548.
(18) Lakowicz, J. R. *Principles of Fluorescence Spectroscopy*, 3rd ed.; Springer: New York, 2006.
(19) Ebenstein, Y.; Mokari, T.; Banin, U. *Appl. Phys. Lett.* **2002**, *80*, 4033−4035.
(20) Yao, J.; Larson, D. R.; Vishwasrao, H. D.; Zipfel, W. R.; Webb, W. W. *Proc. Natl. Acad. Sci. U.S.A.* **2005**, *102*, 14284−14289.
(21) Brokmann, X.; Coolen, L.; Dahan, M.; Hermier, J. P. *Phys. Rev. Lett.* **2004**, *93*, 107403.
(22) Nirmal, M.; Dabbousi, B. O.; Bawendi, M. G.; Macklin, J. J.; Trautman, J. K.; Harris, T. D.; Brus, L. E. *Nature* **1996**, *383*, 802−804.
(23) Ajiki, H.; Ando, T. *Physica B* **1994**, *201*, 349−352.
(24) Islam, M. F.; Milkie, D. E.; Kane, C. L.; Yodh, A. G.; Kikkawa, J. M. *Phys. Rev. Lett.* **2004**, *93*, 037404.
(25) Lefebvre, J.; Homma, Y.; Finnie, P. *Phys. Rev. Lett.* **2003**, *90*, 217401.
(26) Leatherdale, C. A.; Woo, W.-K.; Mikulec, F. V.; Bawendi, M. G. *J. Phys. Chem. B* **2002**, *106*, 7619−7622.
(27) Yu, W. W.; Qu, L.; Guo, W.; Peng, X. *Chem. Mater.* **2003**, *15*, 2854−2860.
(28) Tsay, J. M.; Pflughoefft, M.; Bentolila, L. A.; Weiss, S. *J. Am. Chem. Soc.* **2004**, *126*, 1926−1927.
(29) McBride, J.; Treadway, J.; Feldman, L. C.; Pennycook, S. J.; Rosenthal, S. J. *Nano Lett.* **2006**, *6*, 1496−1501.
(30) Langmore, J.; Wall, J.; Isaacson, M. *Optik* **1973**, *38*, 335−350.
(31) Nair, N.; Usrey, M. L.; Kim, W.-J.; Braatz, R. D.; Strano, M. S. *Anal. Chem.* **2006**, *78*, 7689−7696.
(32) Zheng, M.; Diner, B. A. *J. Am. Chem. Soc.* **2004**, *126*, 15490−15494.
(33) Saito, R.; Dresselhaus, G.; Dresselhaus, M. S. *Physical Properties of Carbon Nanotubes*, 1st ed.; Imperial College Press: London, 1998.
(34) Wang, F.; Dukovic, G.; Brus, L. E.; Heinz, T. F. *Phys. Rev. Lett.* **2004**, *92*, 177401.
(35) Huang, X.; Mclean, R. S.; Zheng, M. *Anal. Chem.* **2005**, *77*, 6225−6228.
(36) Attal, S.; Thiruvengadathan, R.; Regev, O. *Anal. Chem.* **2006**, *78*, 8098−8104.
(37) Berciaud, S.; Cognet, L.; Poulin, P.; Weisman, R. B.; Lounis, B. *Nano Lett.* **2007**, *7*, 1203−1207.
(38) Fagan, J. A.; Simpson, J. R.; Bauer, B. J.; De Paoli Lacerda, S. H.; Becker, M. L.; Chun, J.; Migler, K. B.; Hight Walker, A. R.; Hobbie, E. K. *J. Am. Chem. Soc.* **2007**, *129*, 10607−10612.
(39) Cognet, L.; Tsyboulski, D. A.; Rocha, J.-D. R.; Doyle, C. D.; Tour, J. M.; Weisman, R. B. *Science* **2007**, *316*, 1465−1468.
(40) Paredes, J. I.; Burghard, M. *Langmuir* **2004**, *20*, 5149−5152.
(41) Dukovic, G.; White, B. E.; Zhou, Z.; Wang, F.; Jockusch, S.; Steigerwald, M. L.; Heinz, T. F.; Friesner, R. A.; Turro, N. J.; Brus, L. E. *J. Am. Chem. Soc.* **2004**, *126*, 15269−15276.
(42) Heller, D. A.; Mayrhofer, R. M.; Baik, S.; Grinkova, Y. V.; Usrey, M. L.; Strano, M. S. *J. Am. Chem. Soc.* **2004**, *126*, 14567−14573.
(43) Spataru, C. D.; Ismail-Beigi, S.; Benedict, L. X.; Louie, S. G. *Phys. Rev. Lett.* **2004**, *92*, 077402.
(44) Perebeinos, V.; Tersoff, J.; Avouris, P. *Nano Lett.* **2005**, *5*, 2495−2499.
(45) Zhao, H.; Mazumdar, S. *Phys. Rev. Lett.* **2004**, *93*, 157402.
(46) Shaver, J.; Kono, J.; Portugall, O.; Krstic, V.; Rikken, G. L. J. A.; Miyauchi, Y.; Maruyama, S.; Perebeinos, V. *Nano Lett.* **2007**, *7*, 1851−1855.
(47) Metzger, W. K.; McDonald, T. J.; Engtrakul, C.; Blackburn, J. L.; Scholes, G. D.; Rumbles, G.; Heben, M. J. *J. Phys. Chem. C* **2007**, *111*, 3601−3606.

NL072014+